Available online at www.sciencedirect.com
ScienceDirect
Journal of Sound and Vibration 315 (2008) 343–364
JOURNAL OF SOUND AND VIBRATION
www.elsevier.com/locate/jsvi

On noise robustness of the Mexican-hat and hyperbolic wavelets with an experiment on chaos detection

Khoa N. Le

Griffith School of Engineering, Centre for Wireless Monitoring and Applications, Griffith University, Gold Coast Campus, Queensland, Australia

Received 23 March 2007; received in revised form 22 January 2008; accepted 26 January 2008
Handling Editor: L.G. Tham
Available online 12 March 2008

Abstract

This paper studies the noise robustness of Laplace of hyperbolic (LoH) and Laplace of Gaussian (LoG) wavelets. A typical example of using the LoH and LoG to study Duffing oscillation under normal and noisy conditions is given. Relative merits of each method are discussed.

1. Introduction

Time–frequency signal processing has been the central part in the field of signal processing for many decades. A typical time–frequency distribution is the general distribution defined by Cohen [1,2] in which a kernel plays an important part in shaping the characteristics of the distribution. Kernel design has been an interesting research topic for many years with popular kernels such as Wigner-Ville and Choi–Williams (CW) finding many applications in other fields of science, especially the latter [1–7]. It was found that the CW kernel is the Laplace of Gaussian (LoG), which can be used to generate the popular Mexican-hat wavelet by taking the negative second derivative of the Gaussian pulse. Using the same principle, a hyperbolic wavelet or Laplace of hyperbolic (LoH) was generated from a hyperbolic kernel which was also shown to be more effective in term of noise robustness and cross-term suppression than the popular CW kernel, but less effective in auto-term support in the time–frequency plane [8–11]. To compare kernels in terms of noise robustness and auto-term support, it is necessary to study their auto-term functions, which can be considered as proportional to the noise robustness of the kernel. The method of using the auto-term function has been pioneered by Amin [12], and Stankovic and Ivanovic [13] with foundational works on estimating kernel noise variance.

Time–frequency kernels are two-variable functions of θ and τ, which must meet certain criteria to be valid in Cohen's time–frequency distribution [1,2]. One main problem in time–frequency power spectra of multi-component signals is the coupling of cross terms in the time–frequency plane or also known as artefact which are undesirable. By using an appropriate kernel, its time–frequency distribution can become more efficient

E-mail address: K.Le@griffith.edu.au

0022-460X/$ - see front matter © 2008 Elsevier Ltd. All rights reserved.
doi:10.1016/j.jsv.2008.01.058

with less cross terms and more auto-terms which represent the true time–frequency power spectrum of the input signals. However, even though cross terms are undesirable, it is not possible to completely eliminate them since they form part of the time–frequency power spectrum. Thus, the more auto-terms a power spectrum has, the less artefact and hence the better the representation. Auto-terms in a time–frequency power spectrum are located along straight lines passing through the origin at different angles. Thus, it is possible to detect them by sweeping through the entire time–frequency plane at a fine-enough resolution, i.e. replacing θ with $(a\tau)$ where a is an auto-term slope, yielding auto-term functions as functions of τ, the lagging variable, of the kernel. By estimating the auto-term function, it is possible to study noise robustness of kernels, which is very useful in determining the kernel's performance [11].

Recent publications on the hyperbolic kernel have focused on its noise robustness and auto-term function in which detailed comparisons were made with the CW kernel and Mexican-hat wavelet [8–11]. A recent work by Shark and Yu [14] studied the LoG power spectrum by using a generalized LoG. The new matched wavelet, which can be defined by matching the generalized LoG with a polynomial, was shown to be more effective than the LoG by improving peak detection by at least 10% using graphical computer simulations. However, a systematic approach on studying noise robustness of symmetrical wavelets has not been established.

In this paper, motivated by the auto-term method applied to time–frequency kernels, to compare the performance of wavelets, the method of finding wavelet "auto-term functions" is employed which is of the same principle as has been applied to time–frequency kernels. It should be noted that the LoG and LoH are generated by taking the negative second derivative of the corresponding kernels. It should also be stressed that wavelet signal processing is essentially a time–frequency signal processing in which symmetrical wavelets have been rarely used because they are not orthogonal and their scale functions do not exist. However, they are more effective than orthogonal wavelets in detecting matched features and edges in images [15–17]. By providing a benchmark comparison in terms of noise robustness, it is possible to systematically assess performance of symmetrical wavelets under different values of their control parameters such as σ for the LoG and β for the LoH.

This work continues the work on comparing the hyperbolic and CW kernels reported in [3], hyperbolic and CW wavelets [10,18] and on deriving the auto-term and estimating the noise robustness of these two kernels [8]. The lower and upper bounds signal-to-noise ratio of the first- and nth-order hyperbolic kernels have also been studied [14,19]. CW and hyperbolic distributions have also been employed to model the distribution of random scatterers in multi-path mobile environment, from that, the angle-of-arrival probability density function was derived [20,21]. The key objective of this paper is to use the auto-term method, which has been widely used to derive auto-term functions of time–frequency kernels, to approximately estimate the auto-term functions of symmetrical wavelets. The aims of this paper are thus three-fold: (1) to systematically estimate the auto-term functions of the LoG and LoH, and (2) to assess the performance of the LoG and LoH by estimating their noise robustness. In addition, the LoG and LoH are also employed to detect chaos in Duffing oscillation under normal and noisy conditions.

The paper is organized as follows. Section 2 derives the LoG auto-term function with detailed approximations when β is small and when it is large. Section 3 derives the LoH auto-term function with approximations when σ is small (β large) and when it is large (β small). Sections 4.1 and 4.2 qualitatively compare the performance of the LoG and LoH, in which performance comparisons with their corresponding CW and hyperbolic kernels are given. Section 4.3 quantitatively compares the performance of the LoG and LoH under the typical condition of $a\beta = 1$. Sections 5.1 and 5.2 give background on the continuous wavelet power spectra and Duffing oscillation. Sections 5.3–5.6 perform experiments on using the LoG and LoH to study Duffing oscillation under normal and noisy conditions. Section 6 concludes the main findings of the paper and outlines possible further work.

In this paper, the noise robustness of the LoG and LoH is estimated as functions of β and a. The parameter $\omega = 1$ rad/s is employed as was in Ref. [22] to study the Duffing oscillator. Typically, a is in the range of $0.1 \leqslant a \leqslant 10$ [1,12,13], thus, it can be considered that as β approaches infinity (β is large), $\beta \gg a$ and thus a and ω can be safely ignored to simplify theoretical noise robustness expressions. For small β, appropriate approximations can also be obtained. The noise robustness ratio of the LoH to the LoG is also obtained under a typical condition of $a\beta = 1$ in Section 4.3.

2. LoG noise robustness estimation

The CW kernel is given by

$$\Phi_{\mathrm{CW}}(\theta,\tau)=\exp\left(-\frac{\theta^2\tau^2}{\sigma}\right), \tag{1}$$

where σ is the kernel's control parameter.

The LoG is mathematically given by taking the negative second-order derivative of the CW kernel

$$\mathrm{LoG}(\tau)\big|_{\theta=-a\tau}=12\beta a^2\tau^2\exp(-\beta a^2\tau^4)-16\beta^2a^4\tau^6\exp(-\beta a^2\tau^4), \tag{2}$$

with $\sigma=1/\beta$,

The LoG energy is given by

$$\int_{-\infty}^{+\infty}12\beta a^2\tau^2\exp(-\beta a^2\tau^4)-16\beta^2a^4\tau^6\exp(-\beta a^2\tau^4)\mathrm{d}\tau\approx16(\beta^{0.75})a^{1.5}. \tag{3}$$

The LoG auto-term function is therefore given as

$$\text{auto-term of LoG}=\int_{-\infty}^{+\infty}\exp\left(-\frac{a^2\tau^4}{\sigma}\right)\mathrm{e}^{-\mathrm{j}\omega\tau}\,\mathrm{d}\tau. \tag{4}$$

or with $\sigma=1/\beta$ Eq. (4) can be rewritten as

$$\text{auto-term of LoG}=\int_{-\infty}^{+\infty}\exp(-\beta a^2\tau^4)\mathrm{e}^{-\mathrm{j}\omega\tau}\,\mathrm{d}\tau. \tag{5}$$

Using Maple and combining the condition of $\sigma=1/\beta$, and with $\gamma=\beta a^2$, Eq. (5) can be explicitly given as

$$\begin{aligned}\text{LoG auto-term}=&-\frac{96(\gamma)\sqrt{2\pi}}{\omega^2(\gamma)^{0.25}}\left(\begin{array}{c}\dfrac{\sqrt{2}(\omega^2)\Gamma(0.75){}_0F_2\left\{[],\,[0.5,0.25],\dfrac{\omega^4}{256\gamma}\right\}}{32\sqrt{\pi\gamma}}\\ -\dfrac{\sqrt{\pi}\omega^4{}_0F_2\left\{[],\,[1.5,0.75],\dfrac{\omega^4}{256\gamma}\right\}}{128\Gamma(0.75)(\gamma)}\end{array}\right)\\ &+\frac{32768\gamma^2\sqrt{2\pi}}{\omega^6(\gamma)^{0.25}}\left(\begin{array}{c}\dfrac{3\sqrt{2}\Gamma(0.75)(\omega^6){}_1F_3\left\{[1.75],\,[0.5,0.75,0.25],\dfrac{\omega^4}{256\gamma}\right\}}{32768\sqrt{\pi}(\gamma)^{1.5}}\\ -\dfrac{5\sqrt{\pi}\omega^8{}_1F_3\left\{[2.25],\,[1.5,1.25,0.75],\dfrac{\omega^4}{256\gamma}\right\}}{131072\Gamma(0.75)\gamma^2}\end{array}\right).\end{aligned} \tag{6}$$

By letting $z=(\omega^4/256\gamma)=(\omega^4/256\beta a^2)$, the individual hypergeometric terms in Eq. (6) can be mathematically expressed as

$${}_0F_2\{[],\,[0.5,0.25],z\}=\sum_{k=0}^{+\infty}\frac{1}{\dfrac{\Gamma(0.5+k)}{\Gamma(0.5)}\dfrac{\Gamma(0.25+k)}{\Gamma(0.25)}}\frac{z^k}{k!}, \tag{7}$$

$${}_0F_2\{[],\,[0.75,1.5],z\}=\sum_{k=0}^{+\infty}\frac{1}{\dfrac{\Gamma(0.75+k)}{\Gamma(0.75)}\dfrac{\Gamma(1.5+k)}{\Gamma(1.5)}}\frac{z^k}{k!}, \tag{8}$$

$$ {}_1F_3\{[1.75],[0.5,0.75,0.25],z\} = \sum_{k=0}^{+\infty} \frac{\dfrac{\Gamma(1.75+k)}{\Gamma(1.75)}}{\dfrac{\Gamma(0.5+k)}{\Gamma(0.5)}\dfrac{\Gamma(0.75+k)}{\Gamma(0.75)}\dfrac{\Gamma(0.25+k)}{\Gamma(0.25)}}\frac{z^k}{k!}, \tag{9} $$

$$ {}_1F_3\{[2.25],[0.75,1.5,1.25],z\} = \sum_{k=0}^{+\infty} \frac{\dfrac{\Gamma(2.25+k)}{\Gamma(2.25)}}{\dfrac{\Gamma(0.75+k)}{\Gamma(0.75)}\dfrac{\Gamma(1.5+k)}{\Gamma(1.5)}\dfrac{\Gamma(1.25+k)}{\Gamma(1.25)}}\frac{z^k}{k!}, \tag{10} $$

From Eqs. (7)–(10), Eq. (6) can be rewritten as

$$ \begin{aligned} \text{LoG auto-term} = & -(\gamma^{0.25}) \sum_{k=0}^{+\infty} \frac{1}{\dfrac{\Gamma(0.5+k)}{\Gamma(0.5)}\dfrac{\Gamma(0.25+k)}{\Gamma(0.25)}k!} z^k \\ & + \frac{2.72\omega^2 \sum_{k=0}^{+\infty} \dfrac{1}{\dfrac{\Gamma(0.75+k)}{\Gamma(0.75)}\dfrac{\Gamma(1.5+k)}{\Gamma(1.5)}k!} z^k}{(\gamma^{0.25})} \\ & + \frac{2.45(\gamma^{0.25}) \sum_{k=0}^{+\infty} \dfrac{\dfrac{\Gamma(1.75+k)}{\Gamma(1.75)}}{\dfrac{\Gamma(0.5+k)}{\Gamma(0.5)}\dfrac{\Gamma(0.75+k)}{\Gamma(0.75)}\dfrac{\Gamma(0.25+k)}{\Gamma(0.25)}k!} z^k}{8\sqrt{\pi}} \\ & - \frac{0.9\omega^2 \sum_{k=0}^{+\infty} \dfrac{\dfrac{\Gamma(2.25+k)}{\Gamma(2.25)}}{\dfrac{\Gamma(0.75+k)}{\Gamma(0.75)}\dfrac{\Gamma(1.5+k)}{\Gamma(1.5)}\dfrac{\Gamma(1.25+k)}{\Gamma(1.25)}k!} z^k}{(\gamma^{0.25})}. \end{aligned} \tag{11} $$

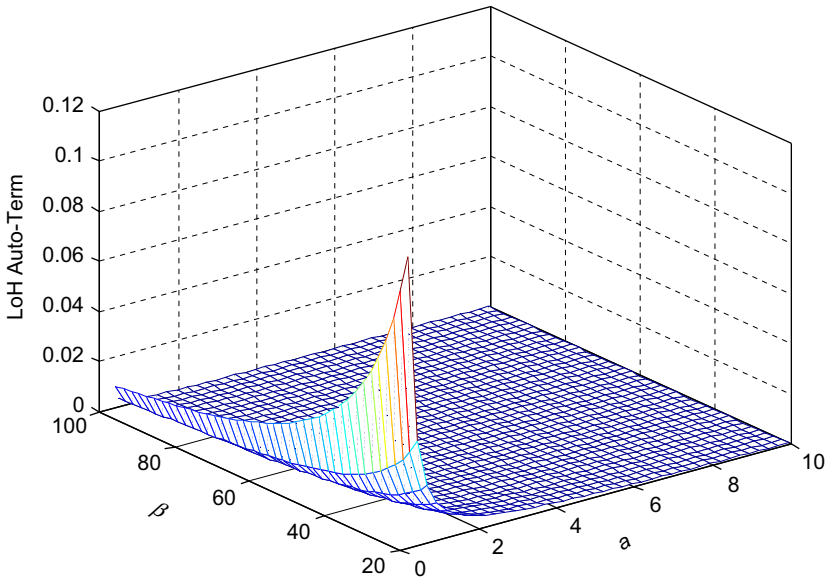

Fig. 1. LoH auto-term as a function of β and a using Eq. (29).

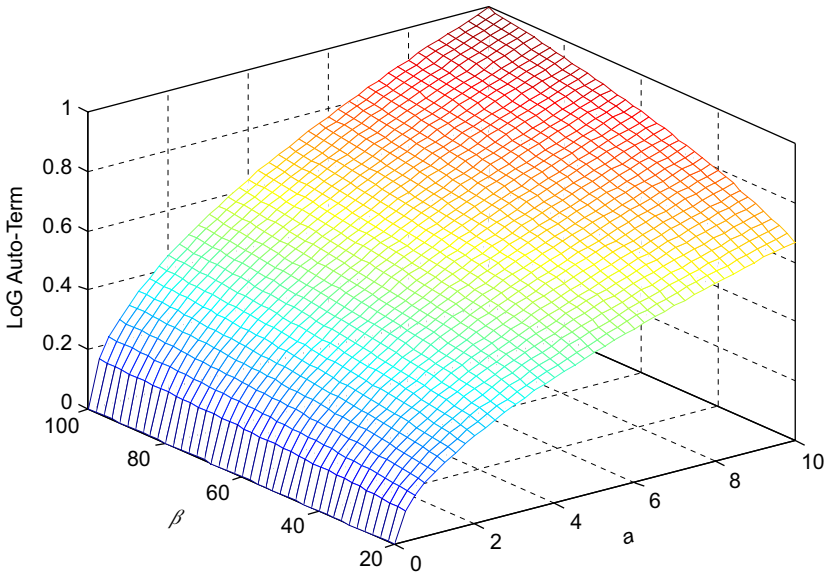

Fig. 2. LoG auto-term as a function of β and a using Eq. (12).

2.1. For large β

Since $0.1 \leqslant a \leqslant 10$ and $\omega = 1$ rad/s [11], when β approaches infinity, z approaches zero, γ approaches infinity, the only dominant term in the infinite summation in Eq. (11) is that corresponding to $k = 0$, yielding

$$\begin{aligned}\text{auto-term of LoG} &= -\gamma^{0.25} + \frac{2.72\omega^2}{\gamma^{0.25}} + 2.45\gamma^{0.25} - \frac{0.9\omega^2}{\gamma^{0.25}} \\ &= 1.45\gamma^{0.25} + \frac{1.82\omega^2}{\gamma^{0.25}} \overset{\gamma\to\infty}{\longrightarrow} 1.45\gamma^{0.25} = 1.45(\beta a^2)^{0.25} = 1.45(\beta^{0.25} a^{0.5}).\end{aligned} \tag{12}$$

By comparing Eq. (12) with Eq. (29), it is clear that the LoG yields a better auto-term value than the LoH as evidenced in Figs. 1 and 2 when β approaches infinity.

2.2. For small β

For small β, z becomes large, therefore $z^k/k!$ will be dominant for small-enough values of k. The LoG auto-term function can then be written as

$$\begin{aligned}\text{LoG auto-term} = \frac{2.72\omega^2}{\gamma^{0.25}} \sum_{k=0}^{+\infty} \frac{1}{\dfrac{(k-0.25)!}{1.2245416}\dfrac{(0.5+k)!}{0.5\sqrt{\pi}}} \frac{z^k}{k!} \\ - \frac{0.9\omega^2}{\gamma^{0.25}} \sum_{k=0}^{+\infty} \frac{\dfrac{(1.25+k)!}{1.133}}{\dfrac{(k-0.25)!}{1.225416}\dfrac{(0.5+k)!}{0.5\sqrt{\pi}}\dfrac{\Gamma(0.25+k)}{0.9064}} \frac{z^k}{k!}\end{aligned}$$

$$= \frac{\omega^2}{\gamma^{0.25}} \left(\sum_{k=0}^{+\infty} \frac{3}{[(k-0.25)!][(0.5+k)!]k!} z^k - \sum_{k=0}^{+\infty} \frac{0.782[(1.25+k)!]}{[(k-0.25)!][(0.5+k)!][(0.25+k)!]k!} z^k \right)$$

$$= \frac{\omega^2}{\gamma^{0.25}}(X - Y). \tag{13}$$

For a large value of z, say $z = 10^6 = \omega^4/(256\gamma)$, which means $\omega^2 = 16{,}000(a\beta^{0.5})$, Eq. (13) becomes

$$\text{LoG auto-term} = 16{,}000a^{0.5}\beta^{0.25} \left[\sum_{k=0}^{+\infty} \frac{3}{[(k-0.25)!][(k+0.5)!]} \frac{(10)^{6k}}{k!} - \sum_{k=0}^{+\infty} \frac{0.782[(k+1.25)!]}{[(k-0.25)!][(k+0.5)!][(k+0.25)!]} \frac{(10)^{6k}}{k!} \right]$$

$$= 6.8476 \times 10^{132} a^{0.5}\beta^{0.25}. \tag{14}$$

From Eq. (14), it is evident that for small β different from 0 which corresponds to large σ, the LoG possesses a large auto-term value which significantly improves its noise robustness. It should be noted that if $\beta = 0$, i.e. $\sigma = +\infty$, then the LoG auto-term is exactly zero which makes it vulnerable to noise.

2.3. Validation

To validate the approximations performed in Sections 2.1 and 2.2, quantitative measures should be taken by estimating the relative errors between the theoretical auto-term expression (Eq. (11)) and the approximated expression (Eq. (12)). Fig. 3 shows the Gaussian auto-term comparison errors for large and small γ. As can be seen from Fig. 3(a), the error becomes small when γ increases which validate the approximation performed in Section 2.1. For small γ, the error is non-zero, however, its magnitude is finite which shows that the

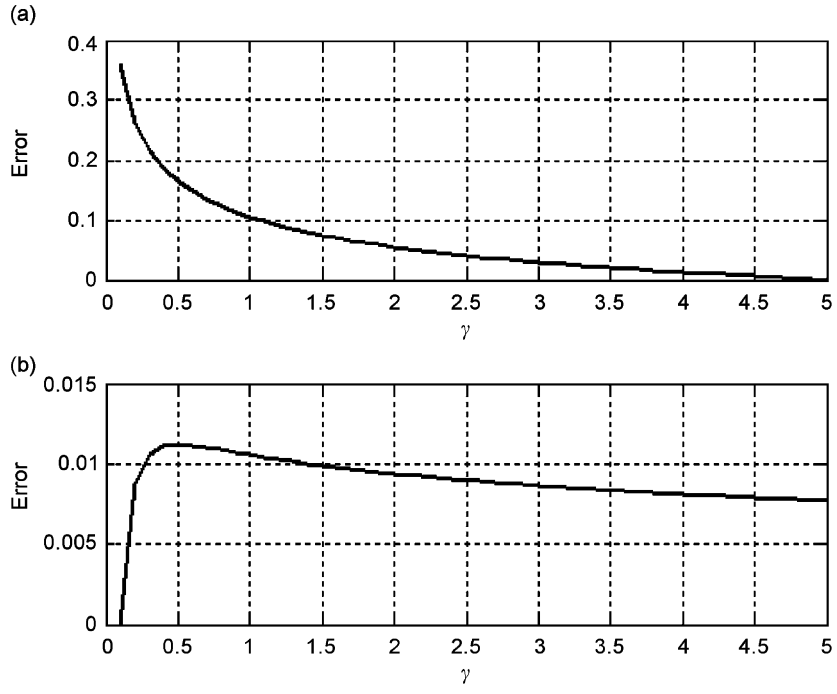

Fig. 3. Gaussian auto-term comparison errors between the theoretical and approximated expressions for large and small γ.

approximation under the large γ condition can be marginally applied under the small γ condition. Similar, from Fig. 3(b), the error rises to about 0.01 when $\gamma \approx 0.5$ and saturates at a final value of about 0.007 when γ is large. Thus, Fig. 3(b) can be used to validate the approximation performed in Section 2.2. It should also be noted that the error magnitude for large and small γ is relatively small which indicates that the approximation is not only correct but also robust which further suggests that the auto-term method of assessing symmetrical wavelets is appropriate.

3. Estimating the LoH noise robustness

The LoH noise robustness is defined as the ratio of its auto-term function and energy. To estimate the LoH auto-term function, its mathematical expression should be generated by taking the kernel's negative second derivative. The hyperbolic kernel is given as

$$H = \operatorname{sech}(\beta\theta\tau), \tag{15}$$

where β is the kernel's control parameter, θ and τ variables in the frequency- and time domain respectively.

The auto-term function of a kernel is defined as

$$\text{auto-term function} = \int_{-\infty}^{+\infty} \Phi(\theta,\tau)\big|_{\theta=-a\tau}\, \mathrm{e}^{-\mathrm{j}\omega\tau}\, \mathrm{d}\tau, \tag{16}$$

where $\Phi(\theta, \tau)$ is the kernel function and a the auto-term slope. By replacing the kernel function $\Phi(\theta, \tau)$ by the mathematical expression of the LoH as given in Eq. (17), the LoH auto-term function can be estimated under specific conditions of β.

The negative second-order derivative of the hyperbolic kernel or LoH as a function of τ is given as

$$\text{LoH} = -\frac{a^2\beta^2\tau^2\{[\cosh(\beta a\tau^2)]^2 - 2\}}{[\cosh(\beta a\tau^2)]^3}. \tag{17}$$

The LoH energy is given by

$$\text{LoH energy} = \left(\int_{-\infty}^{+\infty} \frac{a^2\beta^2\tau^2[\cosh^2(\beta a\tau^2) - 2]}{\cosh^3(\beta a\tau^2)}\, \mathrm{d}\tau\right)^2. \tag{18}$$

The LoH auto-term function is given by

$$\begin{aligned}\text{LoH auto-term} &= \int_{-\infty}^{+\infty} \beta^2 a^2\tau^2\{\operatorname{sech}(\beta a\tau^2) - 2[\operatorname{sech}(\beta a\tau^2)]^3\}\cos(\omega\tau)\,\mathrm{d}\tau \\ &= \beta^2 a^2 \int_{-\infty}^{+\infty} \tau^2 \operatorname{sech}(\beta a\tau^2)\cos(\omega\tau)\,\mathrm{d}\tau - 2\beta^2 a^2 \int_{-\infty}^{+\infty} \tau^2[\operatorname{sech}(\beta a\tau^2)]^3\cos(\omega\tau)\,\mathrm{d}\tau \\ &= A - 2B.\end{aligned} \tag{19}$$

By using the series expansion of $\operatorname{sech}(x)$ [11]

$$\operatorname{sech}(x) = 2\sum_{k=0}^{\infty}(-1)^k \mathrm{e}^{-(2k+1)x}, \quad \text{for } x > 0, \tag{20}$$

Term A in Eq. (19) can be rewritten as

$$A = 2\sum_{k=0}^{+\infty}(-1)^k \int_{-\infty}^{+\infty} \tau^2 \exp[-(2k+1)a\beta\tau^2]\cos(\omega\tau)\,\mathrm{d}\tau, \tag{21}$$

which can be simplified as given in Eq. (22)

$$A = \sqrt{\pi}\sum_{k=0}^{+\infty}(-1)^k\left\{\frac{(4ka\beta + 2a\beta - \omega^2)\exp\left[-\dfrac{\omega^2}{4(2k+1)a\beta}\right]}{2[(2k+1)a\beta]^{5/2}}\right\}. \tag{22}$$

Term B can be rewritten as

$$B = \int_{-\infty}^{+\infty}\tau^2\cos(\omega\tau)\left(2\sum_{k=0}^{+\infty}(-1)^k\exp[-(2k+1)a\beta\tau^2]\right)^3 \mathrm{d}\tau. \tag{23}$$

It should be noted that the auto-term slope a is of a much smaller magnitude order compared to β and ω. Some useful approximations of the LoH auto-term function can be obtained as follows.

3.1. For large β

Only the first two terms of A corresponding to $k = 0$ and 1 are employed because of the dominant term of $\beta^{-2.5}$ in the denominator, from Eq. (22), A can be rewritten as

$$\begin{aligned} A &\approx \sqrt{\pi}\left\{\frac{(2a\beta - \omega^2)\exp\left[-\dfrac{\omega^2}{4a\beta}\right]}{2(a\beta)^{5/2}} - \frac{(6a\beta - \omega^2)\exp\left[-\dfrac{\omega^2}{12a\beta}\right]}{2(3a\beta)^{5/2}}\right\} \\ &= \sqrt{\pi}\left\{\frac{(2\alpha - \omega^2)\exp\left[-\dfrac{\omega^2}{4\alpha}\right]}{2(\alpha)^{5/2}} - \frac{(6\alpha - \omega^2)\exp\left[-\dfrac{\omega^2}{12\alpha}\right]}{2(3\alpha)^{5/2}}\right\}, \end{aligned} \tag{24}$$

where $\alpha = a\beta$.

For Term B, from Eq. (23), only the first term of the infinite series significantly contributes to its value, thus B can be approximately given as

$$B \approx \int_{-\infty}^{+\infty} 8\tau^2\cos(\omega\tau)\exp(-3a\beta\tau^2)\mathrm{d}\tau, \tag{25}$$

which can be simplified to

$$B \approx \frac{2\sqrt{3\pi}(6a\beta - \omega^2)\exp\left(-\dfrac{\omega^2}{12a\beta}\right)}{27(a\beta)^{3/2}}, \tag{26}$$

or

$$B \approx \frac{2\sqrt{3\pi}(6\alpha - \omega^2)\exp\left(-\dfrac{\omega^2}{12\alpha}\right)}{27(\alpha)^{3/2}} \quad \text{with } \alpha = a\beta. \tag{27}$$

The auto-term of the LoH can then be written as

$$\text{LoH auto-term} = A - 2B \approx \frac{\sqrt{\pi}\exp\left(\dfrac{-\omega^2}{12\alpha}\right)\left[6\alpha\exp\left(\dfrac{-\omega^2}{6\alpha}\right) - 3\exp\left(\dfrac{-\omega^2}{6\alpha}\right) - 6\alpha\sqrt{3} + \sqrt{3}\omega^2\right]}{6\alpha^{5/2}}. \tag{28}$$

For small-enough frequency, Eq. (28) can be further simplified as

$$A-2B\approx\frac{\sqrt{\pi}[6\alpha(1-\sqrt{3})-3+\sqrt{3}\omega^2]}{6\alpha^{5/2}}\overset{\alpha\to\infty}{\longrightarrow}\frac{1.3}{\alpha^{3/2}}=\frac{1.3}{(a\beta)^{3/2}}. \tag{29}$$

3.2. For small β

If $\beta=0$, i.e. $\sigma=+\infty$, from Eq. (19), the noise robustness of the LoH is zero which means that it is vulnerable to noise and interferences. To obtain the approximate expression of the LoH auto-term function, it should be noted that only the first terms of Term A and Term B are used because they are the largest in the series. The corresponding Term A and Term B for small β can be given by

$$A=\frac{-\sqrt{\pi}(\omega^2)\exp\left[-\dfrac{\omega^2}{4a\beta}\right]}{2(a\beta)^{5/2}}=\frac{-\sqrt{\pi}(\omega^2)\exp\left(-\dfrac{\omega^2}{4\alpha}\right)}{2\alpha^{5/2}}, \tag{30}$$

and

$$B\approx\frac{-2\sqrt{3\pi}(\omega^2)\exp\left(\dfrac{-\omega^2}{12\alpha}\right)}{27(\alpha)^{3/2}}. \tag{31}$$

Therefore, the LoH auto-term function for small β can be given as

$$A-2B\approx\frac{-\sqrt{\pi}(\omega^2)\exp\left(-\dfrac{\omega^2}{4\alpha}\right)}{2\alpha^{5/2}}+\frac{4\sqrt{3\pi}(\omega^2)\exp\left(\dfrac{-\omega^2}{12\alpha}\right)}{27\alpha^{3/2}}. \tag{32}$$

Because α is small, hence $\alpha^{1.5}$ is much larger than $\alpha^{2.5}$, and for large enough ω, Term B will be much smaller than Term A. Thus, Eq. (32) can be rewritten as

$$A-2B\approx-\frac{0.886(\omega^2)\exp\left(-\dfrac{\omega^2}{4\alpha}\right)}{\alpha^{5/2}}, \tag{33}$$

which is plotted in Fig. 4.

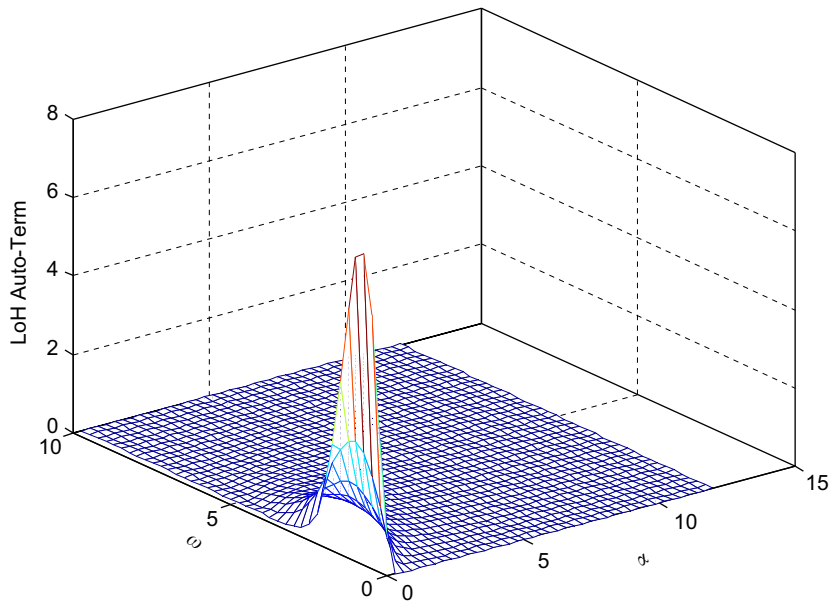

Fig. 4. LoH auto-term as a function of α and ω for small β.

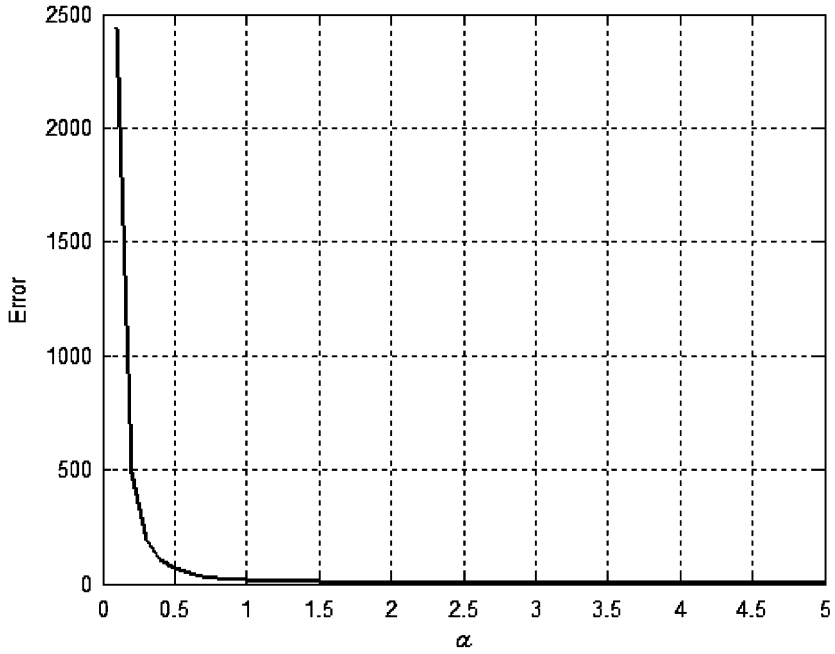

Fig. 5. Hyperbolic auto-term comparison error for large α.

From Eq. (33), it is evident that under DC condition, the LoH auto-term is zero, leading to zero noise robustness. From Fig. 4, for $0<\omega<5$ rad/s, the auto-term function attains its peak. For $\omega>5$ rad/s, the function rapidly decays to zero.

3.3. Validation

Similar to Section 2.3, the relative errors between the theoretical and approximate auto-term expressions for small and large β are estimated in this section to validate the findings reported in Sections 3.1 and 3.2. From Fig. 5, for small α, the error appears to be infinite. However, for large α, the error becomes virtually zero and which validates the approximation performed in Section 3.1. For small α, as shown in Section 3.2, the theoretical hyperbolic auto-term expression is directly employed to compare the effectiveness of the hyperbolic and Gaussian wavelets, therefore, further validation is not required in this case. Because the approximations in Sections 2 and 3 are validated, the findings shown in Section 4 can also be validated.

4. Noise robustness comparison of the LoG and LoH

Using results obtained in Sections 2 and 3, this section aims to compare the noise robustness of the LoH and LoG under different conditions of β, a and ω.

4.1. For large β

The noise robustness ratio R_N of the LoG and LoH is used to compare the performance of the LoG and LoH. The ratio R_N is given as

$$R_N = \frac{\text{LoH noise robustness}}{\text{LoG noise robustness}} = \left(\frac{\text{LoH auto-term function}}{\text{LoG auto-term function}}\right)\left(\frac{\text{LoG energy}}{\text{LoH energy}}\right). \tag{34}$$

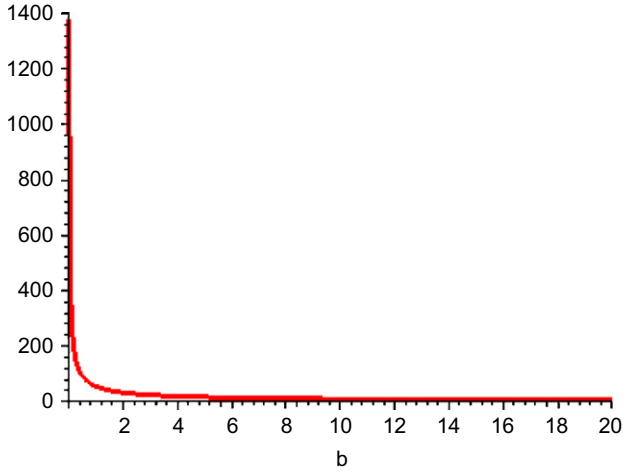

Fig. 6. Energy ratio R_E of the LoG to LoH as a function of $b = \beta a^2$.

The energy ratio R_E of the LoG to LoH is the ratio of Eq. (3) to Eq. (18) and is given by

$$R_E = \frac{16(\beta a^2)^{0.75}}{\left(\int_{-\infty}^{+\infty} \frac{a^2\beta^2\tau^2\{[\cosh(\beta a\tau^2)]^2 - 2\}}{[\cosh(\beta a\tau^2)]^3} \mathrm{d}\tau\right)^2}, \tag{35}$$

which is plotted in Fig. 6.

From Fig. 6, it is clear that the energy ratio of the LoG to LoH is larger than 1 which indicates that the LoH is more noise robustness than the LoG. The auto-term ratio of the LoH to LoG is approximately given by

$$\frac{\text{auto-term of LoH}}{\text{auto-term of LoG}} \approx \frac{1.3}{1.45a^2\beta^{1.75}}. \tag{36}$$

The noise robustness ratio of the LoH to the LoG is therefore given by

$$\begin{aligned} R_N &= \frac{16(\beta a^2)^{0.75}}{\left(\int_{-\infty}^{+\infty} \frac{a^2\beta^2\tau^2\{[\cosh(\beta a\tau^2)]^2 - 2\}}{[\cosh(\beta a\tau^2)]^3} \mathrm{d}\tau\right)^2} \frac{1.3}{1.45a^2\beta^{1.75}} \\ &= \frac{14.34}{a^{4.5}\beta^5\left(\int_{-\infty}^{+\infty} \frac{\tau^2\{[\cosh(\beta a\tau^2)]^2 - 2\}}{[\cosh(\beta a\tau^2)]^3} \mathrm{d}\tau\right)^2}. \end{aligned} \tag{37}$$

It should be clear that when β becomes very large, Eq. (37) approaches zero. However, to further reveal salient features of the noise robustness ratio, Eq. (37) is plotted in Fig. 7 as a function of a and β from which it is evident that the noise robustness ratio of the LoH to the LoG behaves like an impulse centred at around $a = \beta = 0.5$. From Fig. 7, it is evident that the LoH is more effective than the LoG for signals with auto-terms located close to the x and y axes in the time–frequency plane, i.e. a is small.

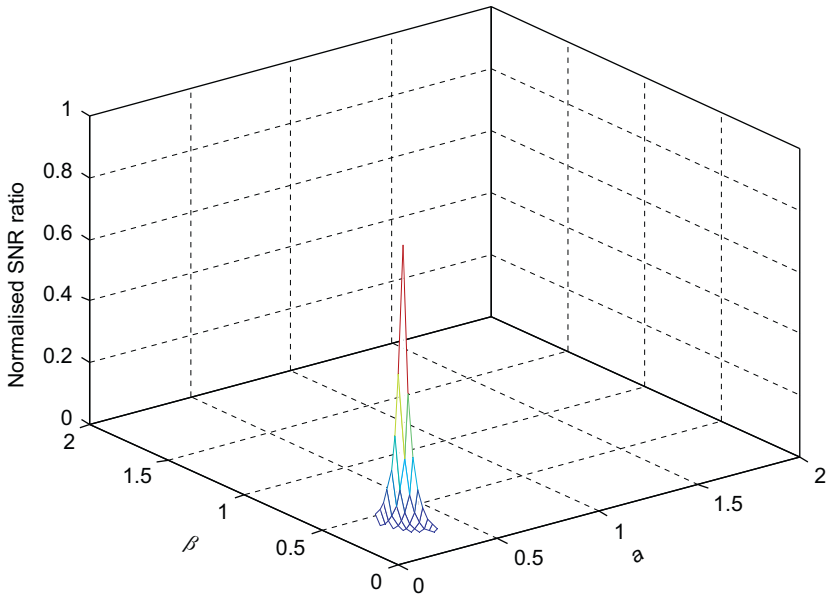

Fig. 7. Normalized noise robustness ratio of the LoH to LoG as a function of β and a for large β.

4.2. For small β

By using Eq. (35) for the energy ratio R_E, and Eqs. (33) and (14), respectively, for the auto-term functions of the LoH and LoG, the noise ratio is given in Eq. (38) as

$$R_N = \frac{16(\beta a^2)^{0.75}}{\left(\int_{-\infty}^{+\infty} \frac{a^2\beta^2\tau^2\{[\cosh(\beta a\tau^2)]^2-2\}}{[\cosh(\beta a\tau^2)]^3}\,\mathrm{d}\tau\right)^2} \left(\begin{array}{l} 0.886(\omega^2)\exp\left(-\dfrac{\omega^2}{4a\beta}\right) \\ \dfrac{(a\beta)^{5/2}}{6.8476\times 10^{132}a^{0.5}\beta^{0.25}} \end{array}\right)$$

$$= \frac{32.375\,\exp\left(-\dfrac{4000}{\beta^{0.5}}\right)}{(10^{129})a^{4.5}\beta^{5.5}\left(\int_{-\infty}^{+\infty} \frac{\tau^2\{[\cosh(\beta a\tau^2)]^2-2\}}{[\cosh(\beta a\tau^2)]^3}\,\mathrm{d}\tau\right)^2} \to 0. \tag{38}$$

Thus, it can be suggested that the LoH is more effective than the LoG for large β. This means that for signals with auto-terms located mainly in the first quadrant of the time–frequency plane, the LoH can be more effectively used because of its superior noise robustness and auto-term support. The inverse proportionality of the signal-to-noise ratio of the LoH to a and β consequently causes the noise robustness ratio of the LoH to the LoG to be inversely proportional to a and β. It is thus clear that the energy ratio of the LoG to the LoH does not have significant effects on their noise robustness which was observed and presented in Ref. [11] in the form of kernel's weighting functions. Based on this, it is possible to numerically estimate the signal-to-noise ratio of the LoH and LoG as functions of a and β.

To compare the auto-term functions of the LoH and LoG, Eqs. (33) and (14) can be used with some chosen values of ω. It should be realised that for $\omega = 1$ rad/s, the LoH auto-term function attains its "minimum value" for $0 < \omega \leqslant 1$ rad/s and is given by

$$\text{auto-term of LoH} = \frac{0.886\,\exp\left(-\dfrac{1}{4\alpha}\right)}{\alpha^{5/2}} = \frac{0.886\,\exp\left(-\dfrac{1}{4a\beta}\right)}{(a\beta)^{5/2}}. \tag{39}$$

It should also be noted that $z=\omega^4/256\gamma=10^6$, hence, $\omega^2=16{,}000(a\beta^{0.5})$. By using $\omega=1\,\text{rad/s}$, one can work out the relationship between a and β which is given by

$$a=\frac{1}{16000\beta^{0.5}}=0.0625\times10^{-3}(\beta^{-0.5}). \tag{40}$$

The LoH to LoG auto-term ratio is therefore given by

$$\frac{\text{Auto-term of LoH}}{\text{Auto-term of LoG}}=\frac{0.886\exp\left(-\dfrac{1}{4a\beta}\right)}{(a\beta)^{5/2}}\quad\frac{1}{6.8476\times10^{132}a^{0.5}\beta^{0.25}}$$

$$=\frac{0.1265\times10^{-132}\exp\left(-\dfrac{1}{4a\beta}\right)}{a^3\beta^{2.75}}=\frac{518.144\times10^{-123}\exp\left(-\dfrac{61,538}{\beta^{0.5}}\right)}{\beta^{1.25}}\to0, \tag{41}$$

which shows the effectiveness of the LoG over the LoH when β becomes very small, $z=10^6$ and $\omega=1\,\text{rad/s}$.

4.3. For $a\beta=1$

The noise robustness ratio of the LoH to the LoG is qualitatively estimated in Sections 4.1 and 4.2 via Eqs. (37)–(41) for large and small β. However, further information on this ratio can be obtained by estimating it as a function of a and β under specific conditions. By varying a and β under the typical condition of $a\beta=1$ [11–13], the noise robustness ratio of the LoH to LoG can be determined and plotted in Fig. 8 from which for a approaches 10, it seems that the noise robustness ratio is approximately saturated at $-100\,\text{dB}$. As β further increases, the ratio gradually decreases which indicates that β is the dominant factor which can be used to adjust the performance of the LoH and LoG, not a, even though, for $a<10$, it can also be used in conjunction with β to obtain satisfactory performance. From Fig. 8, it can be said that the LoH is more noise robust than the LoG when $\beta\leqslant10$. The performance of the LoH is largely independent of the auto-term slope a as it is evident that when a increases, the noise robustness ratio saturates at around 150 dB for small β. For $a>10$ and large β, it seems that the LoH to LoG noise robustness ratio can reach as low as $-150\,\text{dB}$. For $\beta>10$ and small a, the noise robustness ratio seems to saturate at a final value of about 0 dB. It should be noted that

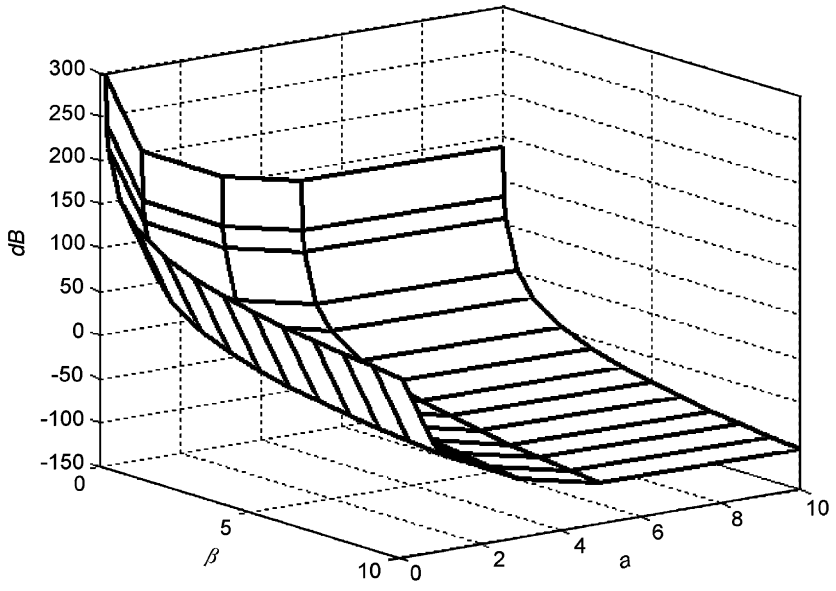

Fig. 8. Noise robustness ratio of the LoH to LoG as a function of β and a, with $a\beta=1$.

Table 1
Performance comparison of time–frequency kernels and their corresponding symmetrical wavelets with $a\beta = 1$

Kernel/wavelet	Noise robustness (dB)	
	Small β	Large β
Hyperbolic kernel	20.3	17.56
Choi–Williams kernel	2585.8 (with $z = 10^6$)	11.9
Hyperbolic wavelet (LoH)	−1.05	2.28
Choi–Williams wavelet (LoG)	2656.7 (with $z = 10^6$)	3.227

Fig. 8 is obtained under the condition of $a\beta = 1$, prompting that new results and insight can be obtained under other conditions.

Table 1 summarizes the links between time–frequency kernels and symmetrical wavelets by comparing their noise robustness when $a\beta = 1$.

5. The use of the LoH and LoG to study Duffing oscillation

In this section, the LoG and LoH power spectra are used to study Duffing oscillation for Period 1, Period 2, Period 4 and chaotic waveforms. Performances of the LoG and LoH under normal and noisy conditions can then be assessed.

5.1. The continuous wavelet power spectrum

The continuous wavelet transform WT(a, b) of an input signal $x(t)$ is defined as [16]

$$\mathrm{WT}(a,b) = \int_{-\infty}^{+\infty} x(t)\psi\left(\frac{t-b}{a}\right)\mathrm{d}t, \tag{42}$$

where a and b are the time and scale indices, respectively, with $\psi(a, b)$ the mother wavelet. In this paper the LoG and LoH are used as mother wavelets so that their noise robustness can be examined.

The wavelet power spectrum WPS(a, b) is defined as [23–25]

$$\mathrm{WPS}(a,b) = [\mathrm{WT}(a,b)][\mathrm{WT}^*(a,b)] = |\mathrm{WT}(a,b)|^2, \tag{43}$$

which is a function of a and b. The WPS can be used to examine characteristics of signals in both time and scale, from which transitions to chaos can also be detected.

5.2. Duffing oscillation

Duffing oscillation is mathematically described by the following equation [22]:

$$\ddot{x} + \delta\dot{x} - 0.5(x - x^3) = F\cos(\omega t), \tag{44}$$

where $\delta = 0.168$, $\omega = 1$ rad/s, and F the driving function. For Period 1, $F_1 = 0.05$; Period 2, $F_2 = 0.178$; Period 4, $F_4 = 0.197$ and for chaotic state, $F_{\mathrm{ch}} = 0.21$. The initial conditions used for the system were $[x \quad \dot{x}] = [0\ 1]$.

5.3. Duffing Period 1

Duffing Period 1 waveform is considered to be purely periodic which is represented by repetitive contours with high energy as can be seen in Fig. 9.

Under random noise of 0.5 dB, the LoG WPS deteriorates in which the main harmonics are partly masked as can be seen in Fig. 10 which clearly shows the existence of background noise. The more background noise, the less robust the wavelet.

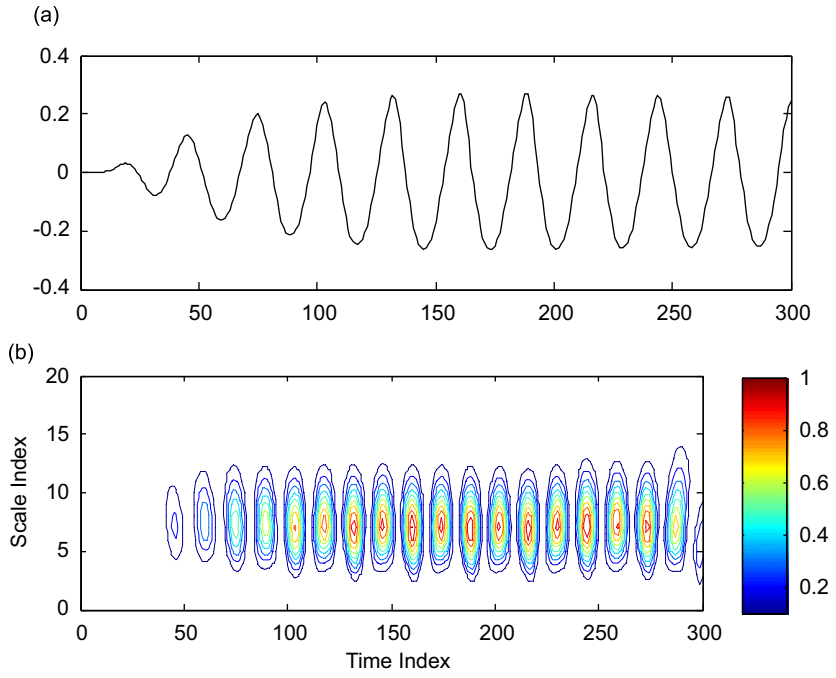

Fig. 9. Duffing Period 1 waveform and its LoG WPS. (a) Duffing period 1 waveform, (b) the WPS_{mexh} of Duffing Period 1 waveform.

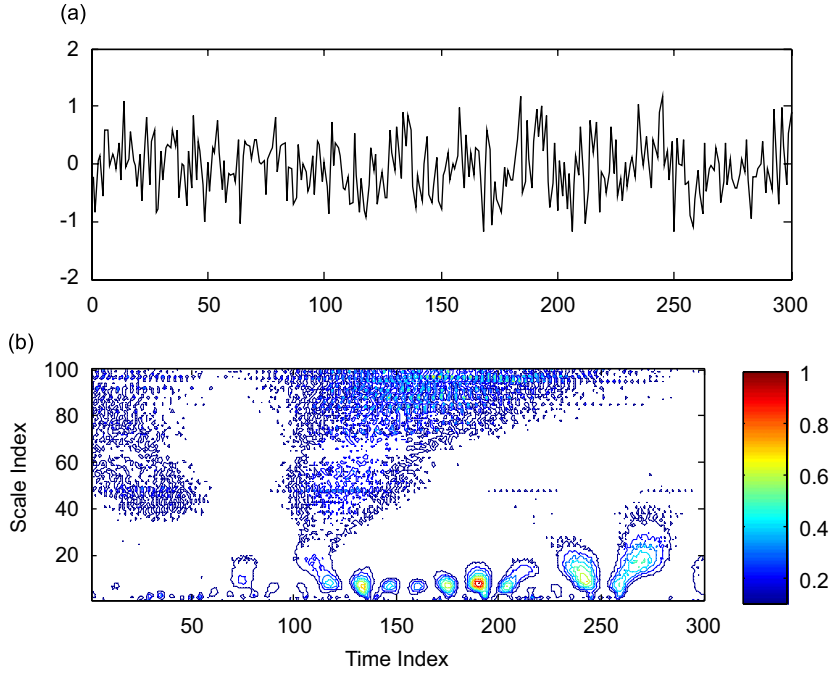

Fig. 10. Duffing Period 1 waveform in random noise of 0.5 dB and its LoG WPS. (a) Duffing Period 1 waveform with added noise, (b) the WPS_{mexh} of noisy Duffing Period 1 waveform.

The LoH WPS is shown in Fig. 11 from which it is clear that the LoH WPS is cleaner than the LoG WPS with less background noise. In addition, even though the waveform is masked by random noise, dominant harmonic peaks can still be recognized which shows that the LoH is more noise robust than the LoG as theoretically shown in Sections 2–4.

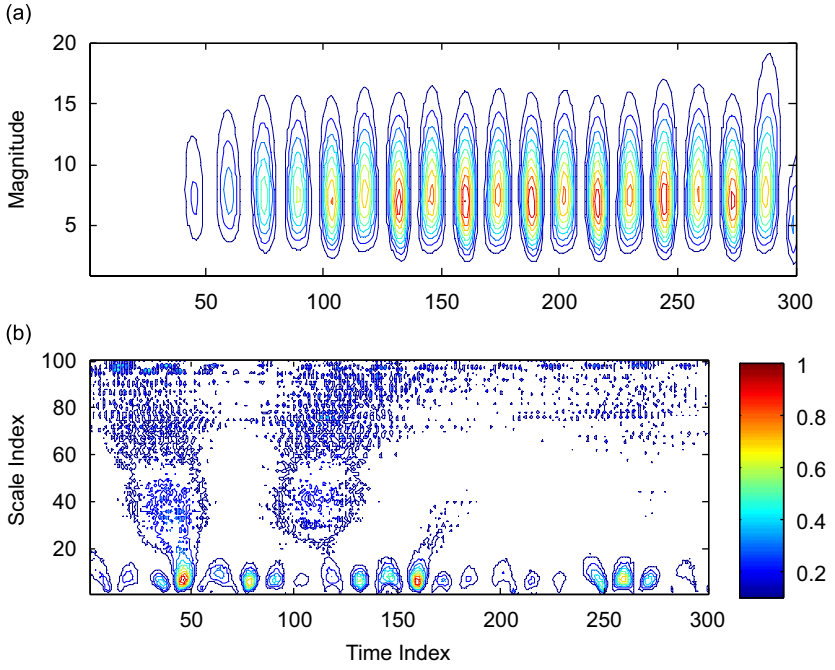

Fig. 11. Duffing Period 1 waveform embedded in random noise of 0.5 dB and its LoH WPS. (a) The WPS_{hyp} of Duffing Period 1 waveform, (b) the WPS_{hyp} of noisy Duffing Period 1 waveform.

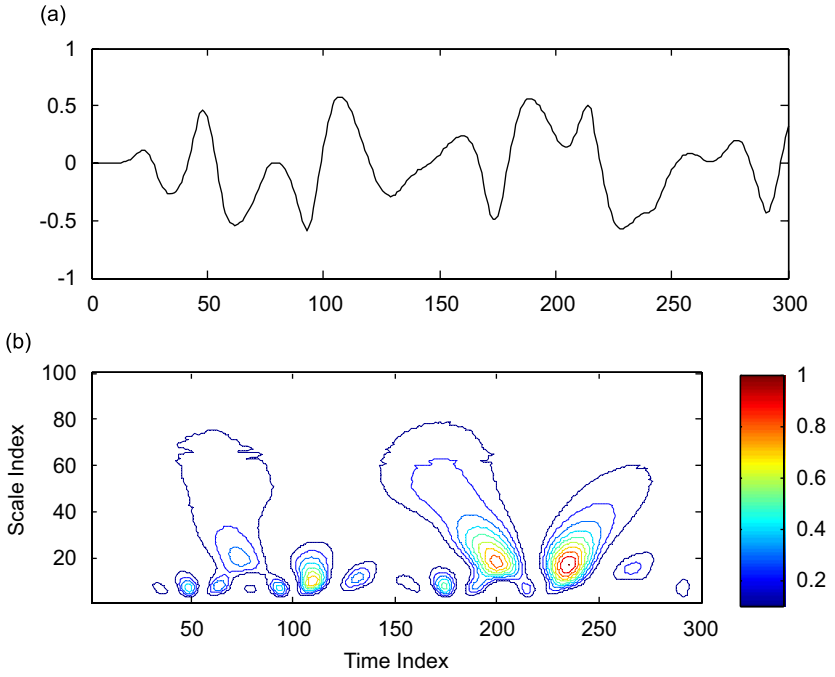

Fig. 12. Duffing Period 2 waveform and its LoG WPS. (a) Duffing Period 2 waveform, (b) the WPS_{mexh} of Duffing Period 2 waveform.

5.4. *Duffing Period 2*

Duffing Period 2 can be considered as similar to Duffing Period 1 except that minor chaotic transition is injected into the waveform which is mainly due to the change of the driving force F as shown in Eq. (44).

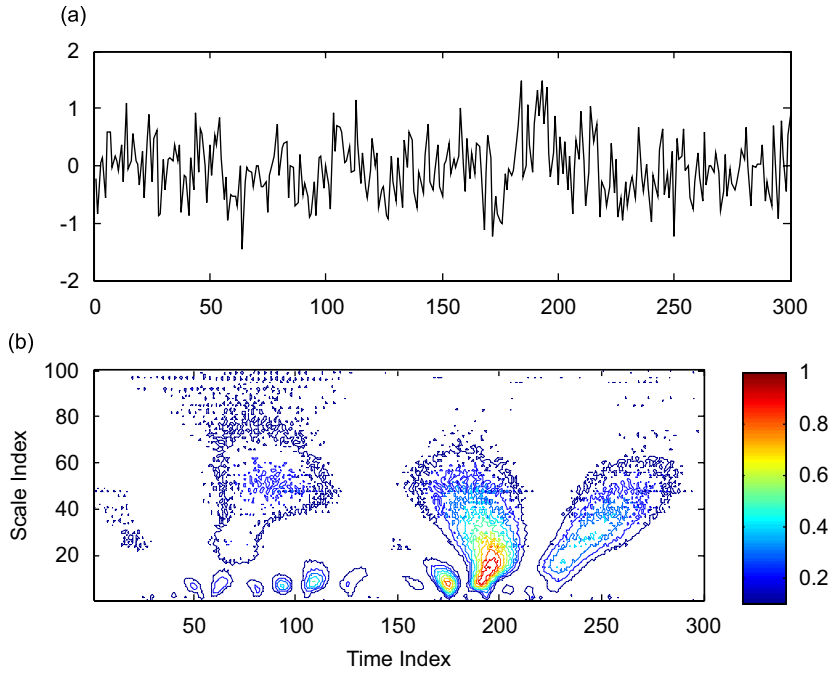

Fig. 13. Duffing Period 2 waveform embedded in random noise of 0.5 dB and its LoG WPS. (a) Duffing Period 2 waveform with added noise, (b) the WPS_{mexh} of noisy Duffing Period 2 waveform.

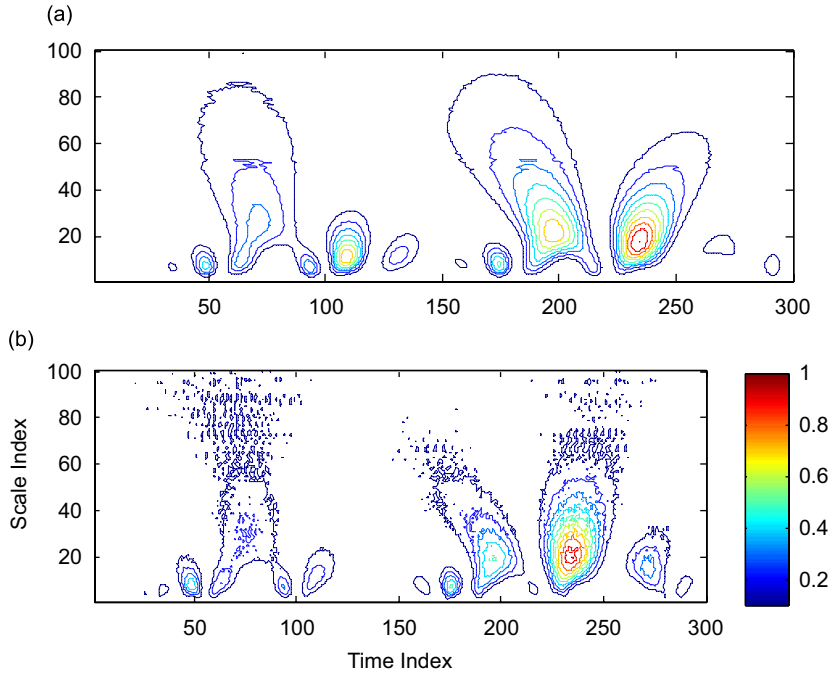

Fig. 14. Duffing Period 2 waveform embedded in random noise of 0.5 dB and its LoH WPS. (a) The WPS_{hyp} of Duffing Period 2 waveform, (b) the WPS_{hyp} of noisy Duffing Period 2 waveform.

Thus it is expected that there are less dominant harmonic peaks. This also means that the energy in the waveform is more broadly distributed than Duffing Period 1 as evidenced in Fig. 12. Fig. 13 shows the LoG WPS of Duffing Period 2 waveform embedded in random noise of 0.5 dB from which it is clear that most

dominant harmonic peaks can clearly be shown. There exists some background noise at high scales (low frequencies). Fig. 14 shows the LoH WPS of Duffing Period 2 embedded in random noise from which it can be suggested that the LoH WPS is slightly cleaner than the LoG WPS. From the findings in Section 5.3, it can be suggested that the LoG performance is improved when the input waveform is not purely periodic. As the nature of the waveform approaches chaos, better noise robustness can be obtained. On the other hand, the LoH noise robustness seems unchanged as the nature of the input waveform deviates from periodicity as can be seen in Fig. 14.

5.5. Duffing Period 4

Duffing Period 4 can be regarded as the transition from periodicity to chaos of Duffing oscillation. As such, it is expected that less harmonic peaks are present in the waveform as evidenced in Fig. 15. Fig. 16 shows the LoG WPS of Duffing Period 4 embedded in random noise of 0.5 dB from which it is evidenced that the LoG WPS is noise robust. There is much less low-frequency background noise which is present in Duffing Period 1, 2 and 4 waveforms. It should be noted that this is consistent with what predicted in Sections 5.4 and 5.5. In addition, the transition from periodicity to chaos of Duffing Period 4 can still be recognized by having contours with broadly distributed energy located at most time indices. Fig. 17 shows the LoH WPS of Duffing Period 4 embedded in random noise of 0.5 dB from which there slightly exists more low-frequency background noise than in the LoG WPS. This shows that the LoG is more noise robust than the LoH for transition-to-chaos waveforms such as Duffing Period 4.

5.6. Duffing chaos

Fig. 18 shows Duffing chaotic waveform and its LoG WPS under normal conditions. Duffing chaotic waveform still possesses dominant harmonic peaks at random intervals. However, it should be noted that this waveform is distinctively different from Duffing Periods 1, 2 and 4 by having broadly distributed contours at low frequencies. These contours are the key differences, which make the waveform to be chaotic. Fig. 19

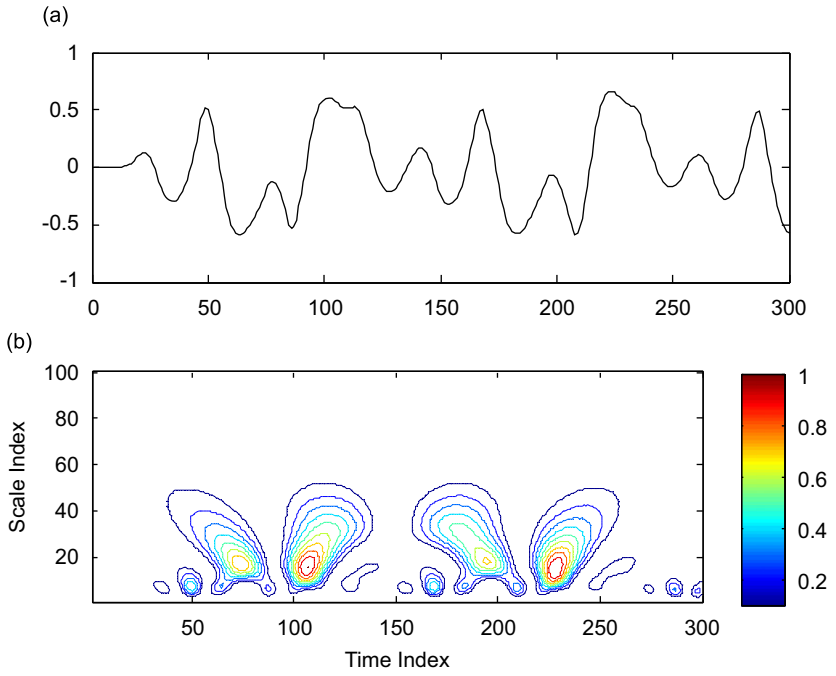

Fig. 15. Duffing Period 4 waveform and its LoG WPS. (a) Duffing Period 4 waveform, (b) the WPS_{mexh} of Duffing Period 4 waveform.

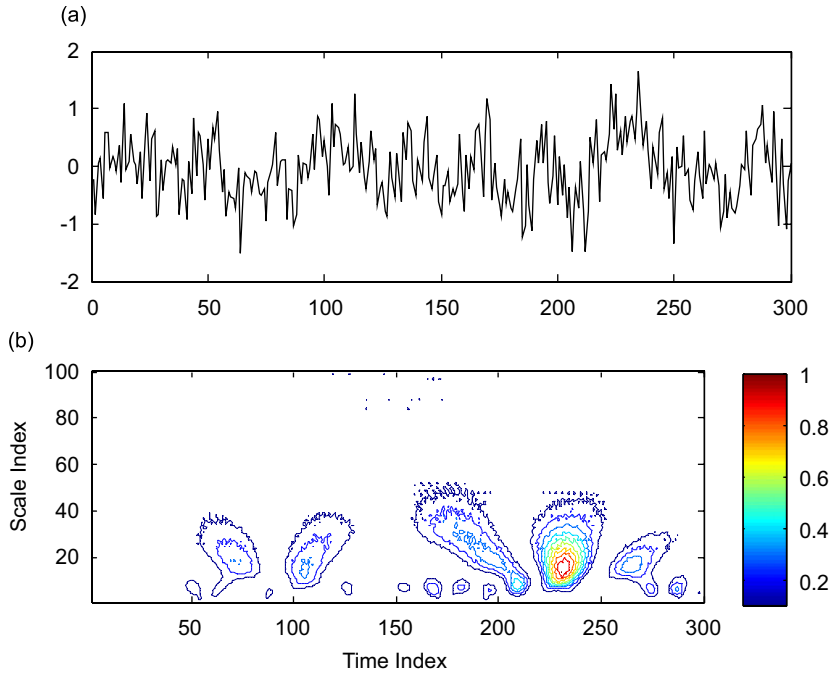

Fig. 16. Duffing Period 4 waveform embedded in random noise of 0.5 dB and its LoG WPS. (a) Duffing Period 4 waveform with added noise, (b) the WPS_{mexh} of noisy Duffing Period 4 waveform.

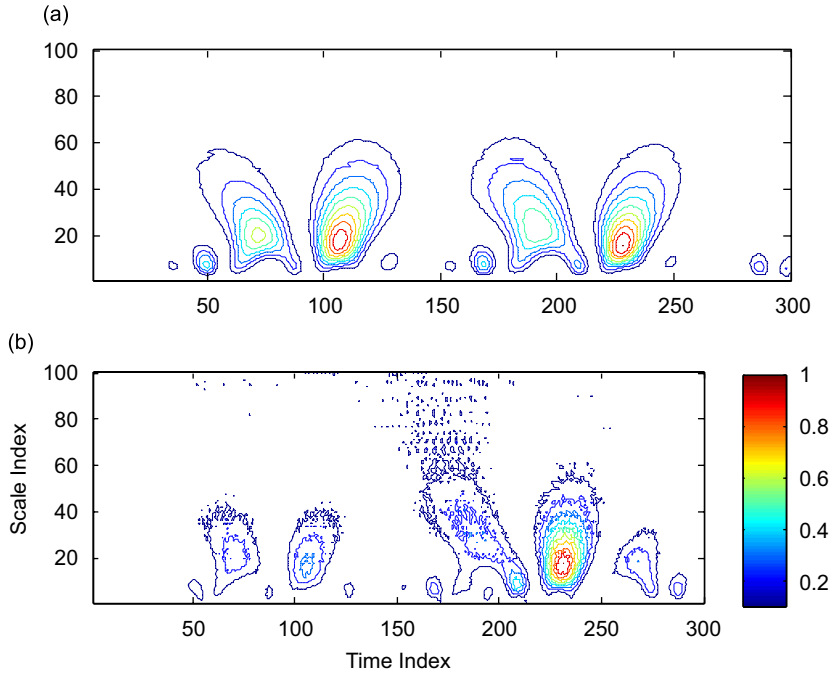

Fig. 17. Duffing Period 4 waveform embedded in random noise of 0.5 dB and its LoH WPS.(a) The WPS_{hyp} of Duffing Period 4 waveform, (b) the WPS_{hyp} of noisy Duffing Period 4 waveform.

graphically shows the LoG WPS in which there exists considerable low-frequency background noise, which suggests that the LoG is not noise robust when the input waveform is purely chaotic. Fig. 20 shows the LoH WPS from which it is clear that the LoH is more noise robust than the LoG for a chaotic input waveform.

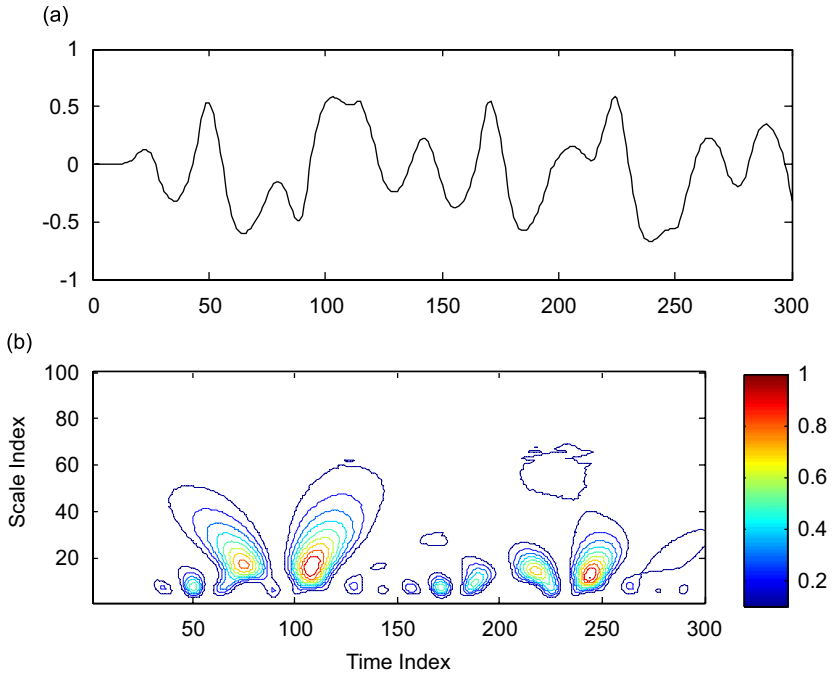

Fig. 18. Duffing chaotic waveform and its LoG WPS. (a) Duffing chaotic waveform, (b) the WPS_{mexh} of Duffing chaotic waveform.

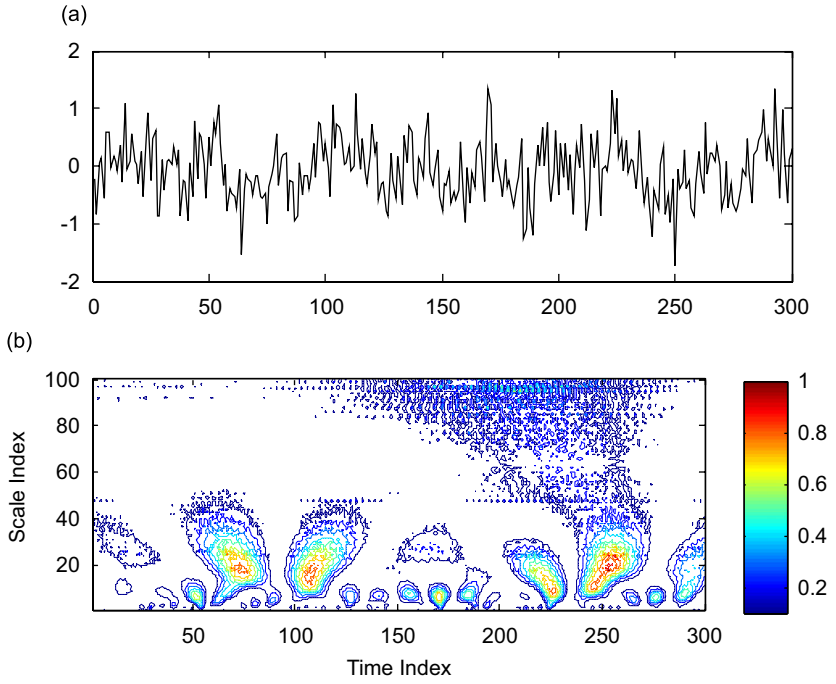

Fig. 19. Duffing chaotic waveform embedded in random noise of 0.5 dB and its LoG WPS. (a) Duffing chaotic waveform with added noise, (b) the WPS_{mexh} of noisy Duffing chaotic waveform.

Another key difference when recognizing periodic and chaotic waveforms is that for the former waveform there exists background noise at all time indices whereas for the latter waveform, the background noise is only present at a few strong harmonic peaks detected by the WPS. From Fig. 19, even though it is possible to detect

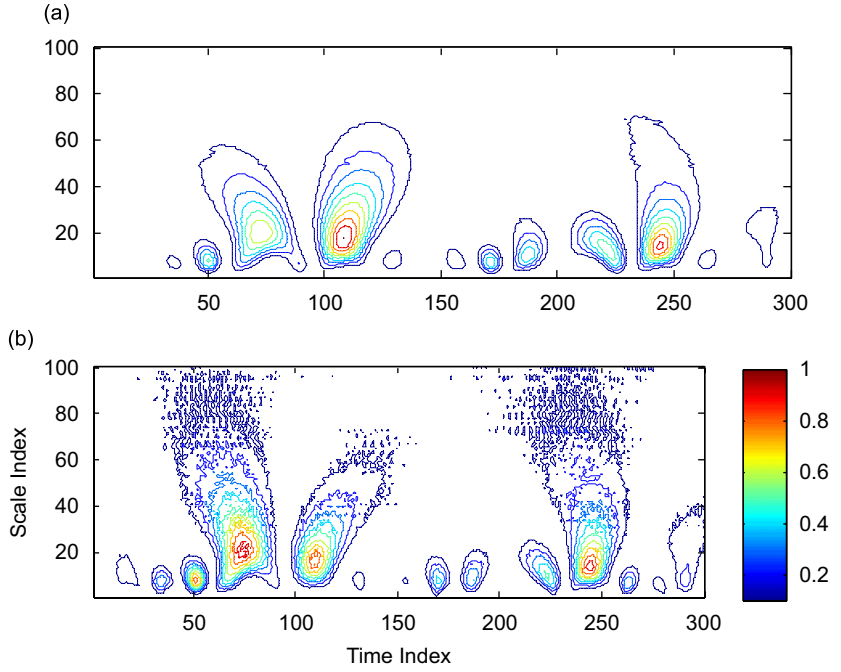

Fig. 20. Duffing chaotic waveform embedded in random noise of 0.5 dB and its LoH WPS. (a) The WPS_{hyp} of Duffing chaotic waveform, (b) the WPS_{hyp} of noisy Duffing chaotic waveform.

chaos in the input waveform, it is clear that the LoG WPS tends to spread the input random noise to other time indices which makes the recognition process more difficult. From Fig. 20, it is clear that the LoH WPS clearly shows distinctive and discontinuous background noise at low frequencies which uniquely represent the chaotic nature of the input waveform.

6. Conclusion and further work

The noise robustness ratio of CW wavelet (LoG) and hyperbolic wavelet (LoH) has been studied in which the LoH was found to perform better than the LoG for large β. For a typical case of $a\beta = 1$, the LoH was found to perform better than the LoG when $\beta \leqslant 10$. Experiments in using the LoG and LoH to study Duffing oscillation have been performed yielding consistent results predicted by theory. It has been shown that the LoG is more noise robust than the LoH for transition-to-chaos input waveforms such as Duffing Period 2 and Period 4. The LoH has been shown to be more effective than the LoG for purely periodic and chaotic waveforms such as Duffing Period 1 and Duffing chaotic. It has also been shown that the LoH WPS can be more effectively used to recognize chaos under noisy conditions in which distinctive and discontinuous background noise can be detected.

Possible further work on the LoG and LoH are as follows:

1. Derivation of a general formula for performance comparisons of the LoH and LoG.
2. Performance dependence on β and the order of derivative used to generate symmetrical wavelets.
3. Performance measures of higher-order symmetrical LoG and LoH for chaotic detection under normal and noisy conditions.

Acknowledgements

The author is grateful to the anonymous reviewer for constructive comments which greatly helped improving the clarity and quality of this manuscript.

References

[1] L. Cohen, Time–frequency distribution—a review, *IEEE Proceedings* 77 (7) (1989) 941–981.
[2] L. Cohen, *Time–Frequency Analysis*, Prentice-Hall, Engle Wood Cliffs, New York, 1995, pp. 136–289.
[3] H.I. Choi, W.J. Williams, Improved time–frequency representation of multi-component signals using exponential kernels, *IEEE Transactions on Signal Processing* 37 (6) (1989) 862–871.
[4] T.A.C.M. Claasen, W.F.G. Mecklenbrauker, The Wigner distribution—a tool of time–frequency signal analysis. Part I: discrete-time signals, *Philips Journal of Research* 35 (3) (1980) 217–250.
[5] T.A.C.M. Claasen, W.F.G. Mecklenbrauker, The Wigner distribution—a tool for time–frequency signal analysis. Part III: relations with other time–frequency signal transformations, *Philips Journal of Research* 35 (6) (1980) 372–389.
[6] T.A.C.M. Claasen, W.F.G. Mecklenbrauker, The Wigner distribution—a tool for time–frequency signal analysis. Part II: continuous-time signals, *Philips Journal of Research* 35 (4–5) (1980) 276–300.
[7] L. Cohen, On a fundamental property of the Wigner distribution, *IEEE Transactions on Acoustics, Speech, and Signal Processing* ASSP-35(4) (1987) 559–561.
[8] K.N. Le, K.P. Dabke, G.K. Egan, Hyperbolic kernel for time–frequency power spectrum, *Optical Engineering* 42 (8) (2003) 2400–2415.
[9] K.N. Le, K.P. Dabke, G.K. Egan, Hyperbolic wavelet power spectra of non-stationary signals, *Optical Engineering* 42 (10) (2003) 3017–3037.
[10] K.N. Le, K.P. Dabke, G.K. Egan, Hyperbolic wavelet family, *Review of Scientific Instruments* 75 (11) (2004) 4678–4693.
[11] K.N. Le, K.P. Dabke, G.K. Egan, On mathematical derivation of auto-term functions and signal-to-noise ratios of Choi–Williams, first- and *n*th-order hyperbolic kernels, *Digital Signal Processing: A Review Journal* 16 (1) (2006) 84–104.
[12] M.G. Amin, Minimum variance time–frequency kernels for signals in additive noise, *IEEE Transactions on Signal Processing* 44 (9) (1996) 2352–2356.
[13] L. Stankovic, V. Ivanovic, Further results on the minimum variance time–frequency distribution kernels, *IEEE Transactions on Signal Processing* 45 (6) (1997) 1650–1655.
[14] L.K. Shark, C. Yu, Design of matched wavelets based on generalized Mexican-hat function, *Signal Processing* 86 (2006) 1451–1469.
[15] P.S. Addison, J.N. Watson, T. Feng, Low-oscillation complex wavelets, *Journal of Sound and Vibration* 254 (4) (2002) 733–762.
[16] C.S. Burrus, R.A. Gopinath, H. Guo, *Introduction to Wavelets and Wavelet Transform: A Primer*, Prentice-Hall, Upper Saddle River, New Jersey, 1998, pp. 1–100.
[17] I. Daubechies, *Ten Lectures on Wavelets*, SIAM, Philadelphia, 1992, pp. 20–100.
[18] K.N. Le, K.P. Dabke, G.K. Egan, *The Hyperbolic Wavelet Function, in SPIE Aerosense Proceedings: Wavelet Applications VIII*, SPIE, Orlando, FL, USA, 2001.
[19] K.N. Le, The Mexican-hat Wavelet and its Applications: A Brief Review, in New Signal Processing Research, 2007, Nova Science Publishing, in press.
[20] K.N. Le, A new formula for the angle-of-arrival probability density function in mobile environment, *Signal Processing* 87 (6) (2007) 1314–1325.
[21] D.D.N. Bevan, et al., Gaussian channel model for mobile multipath environment, *EURASIP Journal on Applied Signal Processing* 2004 (9) (2004) 1321–1329.
[22] J. Guckenheimer, P.J. Holmes, *Nonlinear Oscillators, Dynamical Systems, and Bifurcation of Vector Fields*, Springer, Berlin, 1983.
[23] B.P. van Milligen, C. Hidalgo, E. Sanchez, Nonlinear phenomena and intermittency in plasma and turbulence, *Physical Review Letters* 74 (3) (1995) 395–398.
[24] B.P. van Milligen, et al., Wavelet bicoherence: a new turbulence analysis tool, *Physics of Plasmas* 2 (8) (1995) 3017–3032.
[25] M. Farge, et al., Wavelets and turbulence, *Proceedings of the IEEE* 84 (4) (1996) 639–669.